The effect of the linker group between porphyrin dimers on the thermoelectric properties of molecular junctions

G. Zamel Hassan and M. Deia Noori

Department of Physics, College of Science, University of Thi-Qar, Thi-Qar, Iraq.

Received 28 October 2024; accepted 11 November 2025

The effect of the appearance of three different linkers between dimer porphyrins on the electronic and thermoelectric properties of three different dimer porphyrin families' molecular junctions was investigated theoretically using a combination of density functional theory (DFT) methods. Our results show that in the free-based porphyrin dimer family, all electronic and thermoelectric properties have been affected by using different linkers between porphyrin dimers. While in the presence of one zinc metal ion in the center of the porphyrin dimer and the two zinc metal ion in the center of porphyrin dimer families, the results demonstrate that the electronic and thermal conductance is highly affected by the presence of three different linkers between these dimers. On the other hand, the thermopower of all other structures shows noticeable change, especially around the Fermi energy. Thus, the gradual appearance of zinc ion in the center of porphyrin dimer units with three different linkers between these dimers plays an essential role in these structures' electric and thermal properties.

Keywords: Dimer porphyrin; zinc metal ion; (DFT) method; the thermoelectric figure of merit (ZT).

DOI: https://doi.org/10.31349/RevMexFis.72.030401

1. Introduction

The study of charge transport in molecular junctions (MJs) is pivotal for advancing molecular electronics and thermoelectric [1, 2]. Over the past decade, the thermoelectric properties at the molecular scale have gained significant attention, focusing on the unique behaviors of molecular junctions and organic semiconductors [3]. Understanding thermoelectric effects at the molecular scale is crucial for advancing nanotechnology, particularly as electronic devices shrink to nanometer dimensions [4-6].

The thermoelectric effect creates a voltage across a temperature gradient, converting waste heat into electrical energy [7-12]. Initially proposed in the early nineteenth century, the Seebeck effect is the foundational idea of thermoelectricity [13, 14]. This phenomenon aims to increase the production of electrical current by using the excess heat generated by various industrial processes or the wasted heat in particular physical systems, such as automobile exhausts, by creating an electrical voltage gradient from a thermal gradient [15,16].

Aromatic organic molecules are pivotal in molecular electronics due to their structural versatility and inherent stability, which enable them to perform specific electrical functions. Their conjugated systems facilitate efficient charge transport, making them suitable for various electronic applications [17-20]. Porphyrins are distinguished by their highly conjugated structures, rigid planar geometry, and remarkable chemical stability, which facilitate the formation of metalloporphyrin through metal ion coordination. This unique ability is leveraged across various fields, including materials science, quantum information, and biological systems [21-25].

Among all the metalloporphyrin families, Zinc porphyrins are gaining significant attention due to their remarkable photochemical and photophysical properties, which make them suitable for various applications. Recent studies have highlighted their synthesis, structural characteristics, and potential uses in advanced materials and devices [26-29].

Zinc porphyrin derivatives, in particular, are significant due to their unique structural properties and possible applications in various fields, including catalysis, thermoelectric materials, and spintronics [30]. They have been adjusted for future applications in molecular wires and other nanoelectronics circuits [31], quantum dots [32,33], biological systems[34,35], electrodes [36,37], and switches [38,39]. Research on the thermoelectric properties of zinc porphyrins coupled to gold electrodes produced encouraging findings [40-45].

Investigate the potential for high-efficiency thermoelectricity of porphyrin dimer structures in various configurations. This work examines how the electric and thermoelectric properties of three distinct groups of porphyrin dimers are affected using three different linkers between the dimer units. Each group has a directly linked [46,47], ethynyl-linked[48-52], and phenyl-linked porphyrin dimer [53].

To improve our understanding of how these linkers affect charge transport, electronic characteristics, and thermoelectric performance, it is essential to study zinc porphyrin dimers with free-based configurations, one zinc atom in the center of porphyrin dimer units, and then two zinc atoms in the center of porphyrin dimer units in three different types of linkers between dimer units. These elements are essential for furthering the creation of nanotechnology applications and devices at the molecular level.

2. Methodology

Using quantum physics and quantum chemistry, Density Functional Theory (DFT) is a quantum computational

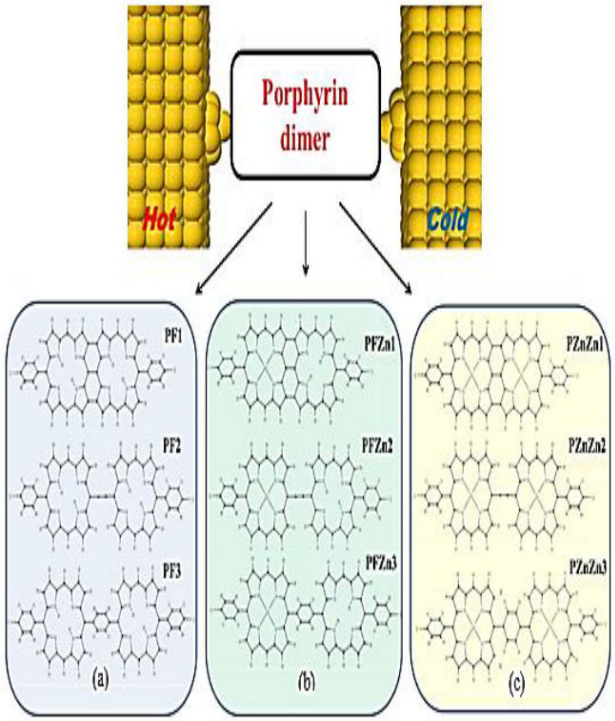

FIGURE 1. Schematic illustration of the molecular structure junctions investigated consists of three different families of zinc porphyrin dimers: a) directly fused free-based porphyrin dimer (PF1), ethynyl-linked free-based porphyrin dimer (PF2), the free-based phenyl-linked porphyrin dimer (PF3), b) directly fused porphyrin dimer with one zinc ion (PFZn1), ethynyl-linked porphyrin dimer with one zinc ion (PFZn2), the phenyl-linked porphyrin dimer with one zinc ion (PFZn3), c) directly fused porphyrin dimer with two zinc ion (PZnZn1), ethynyl-linked porphyrin dimer with two zinc ion (PZnZn2), the phenyl-linked porphyrin dimer with two zinc ion (PZnZn3).

method that employs intricate algorithms to produce geometrical structures across various molecular systems. DFT calculates the electronic properties of multimolecular systems, with the electron density determined by the wave function [54]. All of the molecular structures of the porphyrin trimers, as shown in Fig. 1, were optimized. A double-polarized basis set (DZP) for exchange and correlation [55,56], norm-conserving pseudopotentials, the DFT package SIESTA code [57], a real-space grid defined with an energy cutoff of 200 Rydberg, and the generalized gradient functional approximation (GGA-PBE) were employed for the optimization. We then combine the mean-field Hamiltonian H with the GOLLUM quantum transport code. The mean-field Hamiltonian H and the GOLLUM quantum transport code are integrated to determine the transmission coefficient, $Tel(E)$ [58].

The Landauer formalism is used to express the Seebeck coefficient, which quantifies the crucial role of the transmission $T(E)$ in meeting this requirement for ballistic devices [54].

$$S = -\frac{\Delta V}{\Delta T} = -\frac{1}{eT}\frac{L1}{L0}, \tag{1}$$

where ΔT is established between them, ΔV is the voltage difference generated between the two ends of the junction when temperature difference, e is the electron charge, and L_n can be calculated as

$$L_n = \int_{-\infty}^{\infty} (E - E_F)^n T(E) \left(\frac{\partial f(E,T)}{\partial E}\right) dE, \tag{2}$$

where $f(E,T)$ is the Fermi distribution function defined as

$$f(E,T) = \left(e^{(E-E_F)/K_BT} + 1\right)^{-1},$$

where K_B is *Boltzmann's constant*, from Eq. (1), it can also be obtained that G and K:

$$G = G_0 L_0, \tag{3}$$

where $(G_0 = 2e^2/h)$ is the quantum of conductance,

$$K = \frac{1}{hT}\left(L_2 - \frac{L_1^2}{L_0}\right). \tag{4}$$

This leads to the final evaluation of the figure of merit values (ZT).

$$ZT = S^2 \frac{GT}{K}. \tag{5}$$

3. Results and discussion

To examine the electronic and thermoelectric characteristics of three distinct families of porphyrin dimers with different linkers and various central occupations, as shown in Fig. 1, we begin with the free-base porphyrin dimer featuring three different linkers connecting the porphyrin dimer units. For each structure presented in Fig. 1a), we start by calculating the electrical conductance (G) as an energy function for all free-base porphyrin dimer molecule structures.

Figure 2 shows the essential change in transmission coefficient $T(E)$ when moving from a directly fused freebased

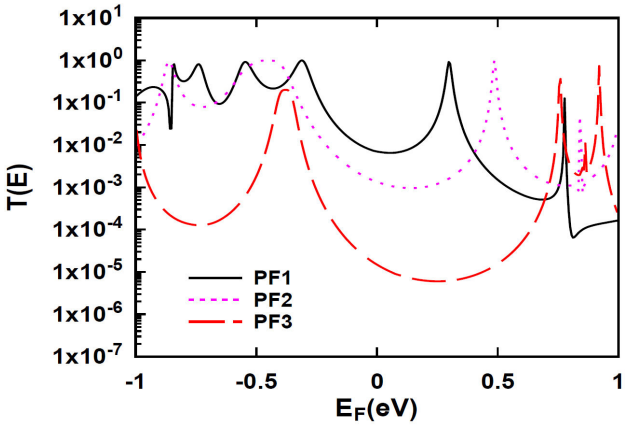

FIGURE 2. The electronic transmission coefficients as a function of energy for all free-based porphyrin dimer molecular structures are presented in Fig. 1a).

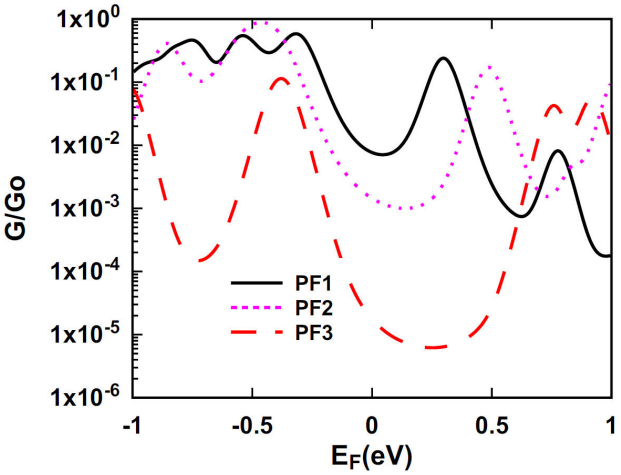

FIGURE 3. The electrical conductance G as a function of energy for all free-based porphyrin dimer molecular structures is presented in Fig. 1a).

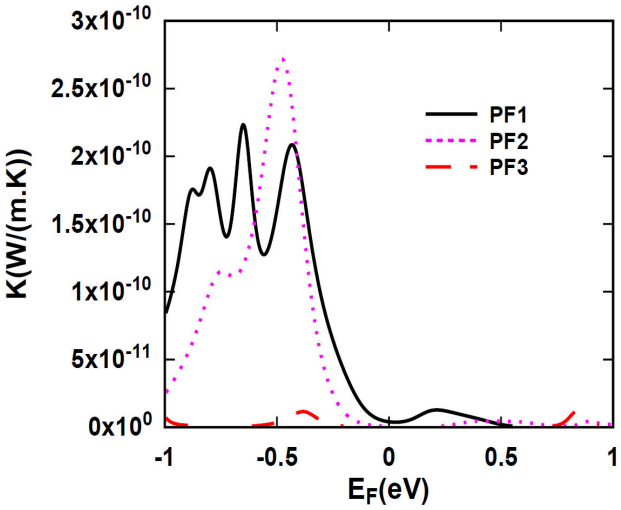

FIGURE 4. The electronic thermal conductivity κ as a function of energy for all free-based porphyrin dimer molecular structures is presented in Fig. 1a).

porphyrin dimer (PF1) (black line) to the freebased phenyl-linked porphyrin dimer (PF3) (red dashed line). This leads to a massive decrease in the transmission coefficient $T(E)$, which is strongly affected by three different linkers between porphyrin dimer units.

The room temperature electrical conductance versus energy is presented in Fig. 3. The electrical conductance decreased with the appearance of a linker of free-base porphyrin dimer units. Figure 3 shows that moving from a directly fused free-based porphyrin dimer (PF1) (black line) to the free-based phenyl-linked porphyrin dimer (PF3) (red dash line) leads to a huge decrease in electrical conductance around Fermi energy, where the electrical conductance follows the trend (PF1)$>$ (PF2) $>$ (PF3) around Fermi energy.

Figure 4 shows the electronic thermal conductivity of these junctions. This figure shows that the electronic thermal conductivity of directly fused free-base porphyrin dimer

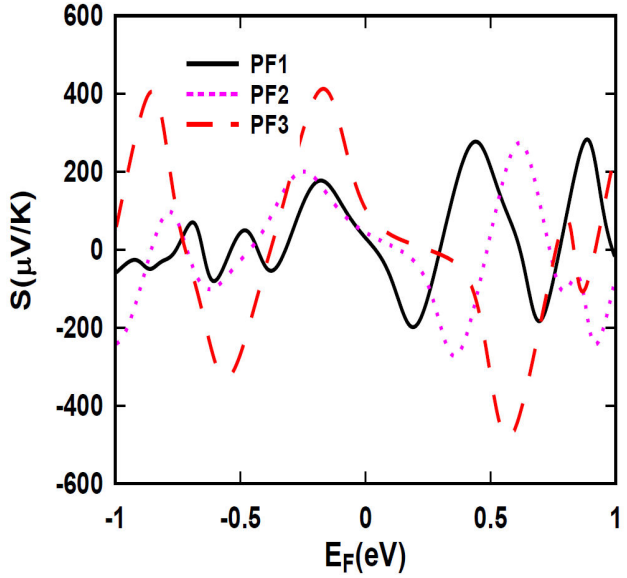

FIGURE 5. The Seebeck coefficient S (thermopower) for all free-based porphyrin dimer molecular structures is presented in Fig. 1a).

(PF1) is higher than that of other structures (PF2) and (PF3). This means that the electronic thermal conductance also decreased with the appearance of a linker between porphyrin dimer units [55,56]. The linkers may disrupt the conjugation or alter the alignment between the porphyrin units, weakening electronic interactions and lowering electron mobility [57,58].

Figure 5 shows the Seebeck coefficient S over a range of Fermi energies at room temperature for each freebased porphyrin dimer. The free-based porphyrin dimer (PF1) has the lowest values (black line), while the freebased phenyl-linked porphyrin dimer (PF3) has the highest values (red dashed line). The phenyl linkers in PF3 provide a favorable conformation that enhances electron mobility and reduces steric hindrance, further optimizing thermoelectric properties.

The essential quantity that determines the thermoelectric efficiency is ZT, which is proportional to the electric conductance G and the square of the Seebeck coefficient S and inversely proportional to the thermal conductance K. For all free-based porphyrin dimers, Fig. 6 shows the thermoelectric figure of merit ZT over a range of Fermi energies at room temperature for each. Due to the highest value of the Seebeck coefficient S and the low value of electronic thermal conductance κ, Fig. 6 shows that the highest thermoelectric figure of merit ZT value is achieved at free-based phenyl-linked porphyrin dimer (PF3).

In the second part of our work, we investigate the impact of the presence of one zinc ion in the center of one of the porphyrin dimer units on the electronic and thermoelectric properties of three different linker porphyrin dimers, as shown in Fig. 1b).

Figure 7 shows the transmission coefficient $T(E)$ as an energy function. The appearance of a single zinc ion in the

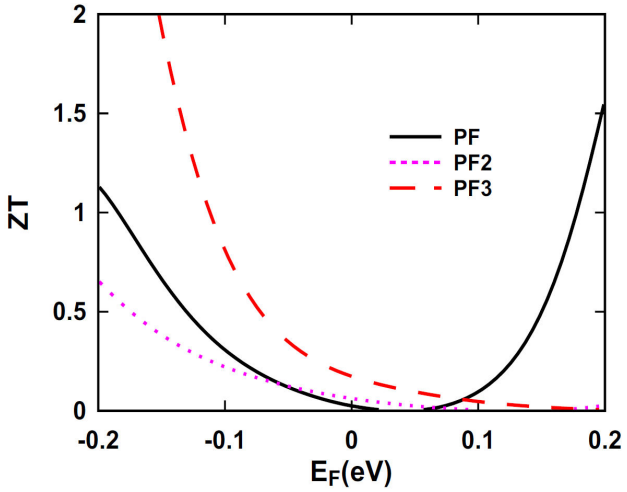

FIGURE 6. The electronic figure of merit ZT for all freebased porphyrin dimer molecular structures is presented in Fig. 1a).

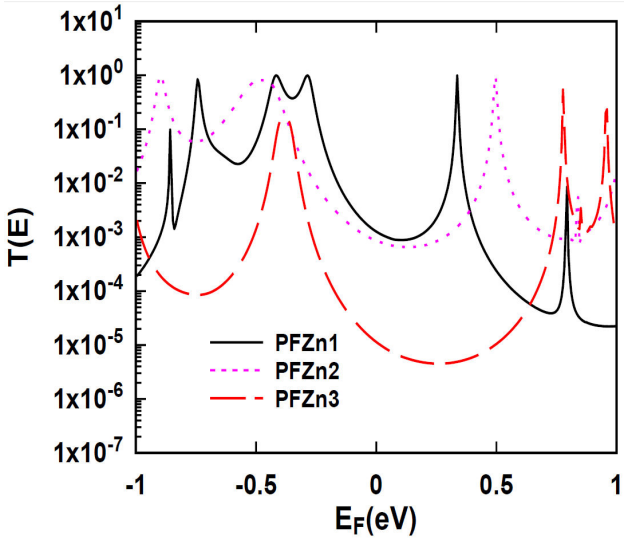

FIGURE 7. The electronic transmission coefficients as a function of energy for a single zinc ion in the centre of porphyrin dimer molecular structures are presented in Fig. 1b).

centre of three different linked porphyrin dimers has a remarkable effect on the transmission coefficient, particularly around the Fermi energy. The appearance of a single zinc ion in the center of porphyrin dimer units leads to shifting the peaks of the transmission coefficient away from the Fermi energy. (black, pink dotted, and red dashed line).

The electrical conductance versus energy is presented in Fig. 8. Figure 8 shows that the electrical conductance decreased with a change in the linker between the porphyrin dimer with one zinc ion unit. Figure 6 shows that moving from the directly fused porphyrin dimer with one zinc ion (PFZn1) (black line) to the phenyl-linked porphyrin dimer with one zinc ion (PFZn3) (red dashed line) leads to a huge decrease in electrical conductance around the Fermi energy. The electrical conductance follows the (PFZn1) $>$ (PFZn2) $>$ (PFZn3) trend around the Fermi energy.

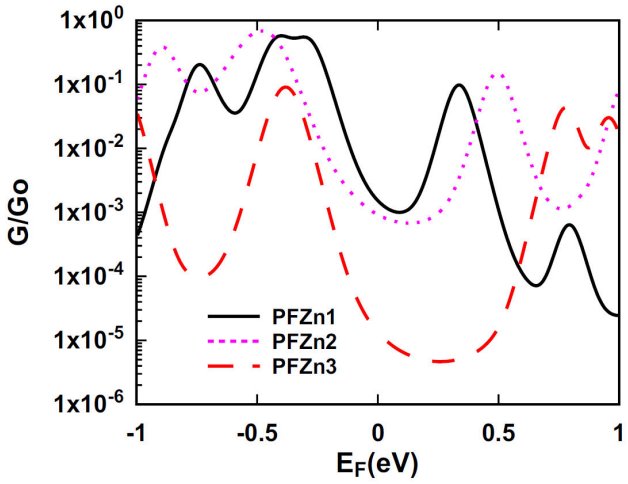

FIGURE 8. The electrical conductance coefficients as a function of energy for a single zinc ion in the center of the porphyrin dimer molecular structures are presented in Fig. 1b).

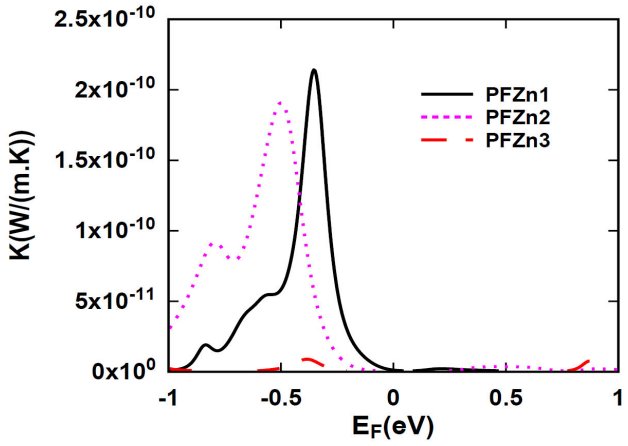

FIGURE 9. The electronic thermal conductivity as a function of energy for a single zinc ion in the center of the porphyrin dimer molecular structures is presented in Fig. 1b).

Figure 9 shows the electronic thermal conductivity of these junctions. Like electrical conductance G, Fig. 9 shows that the electronic thermal conductivity decreases with porphyrin dimer units as the linker changes. The electronic thermal conductivity of directly fused porphyrin dimers with one zinc ion (PFZn1) is higher than that of the others in (PFZn2) and (PFZn3).

Figure 10 shows the Seebeck coefficient S over a range of Fermi energies at room temperature for each porphyrin dimer. Where curves of the Seebeck coefficient S of structures directly fused porphyrin dimer with one zinc ion (PFZn1) and phenyl-linked porphyrin dimer with one zinc ion (PFZn3) are very close, particularly around Fermi energy in energy windows of -0.1 to $+0.1$ eV, the Seebeck coefficient S of structure ethynyl-linked porphyrin dimer with one zinc ion (PFZn2) is the lowest. The synergy between molecular design, zinc's electronic modulation, and optimized carrier dynamics enables both (PFZn1) and (PFZn3) to achieve high

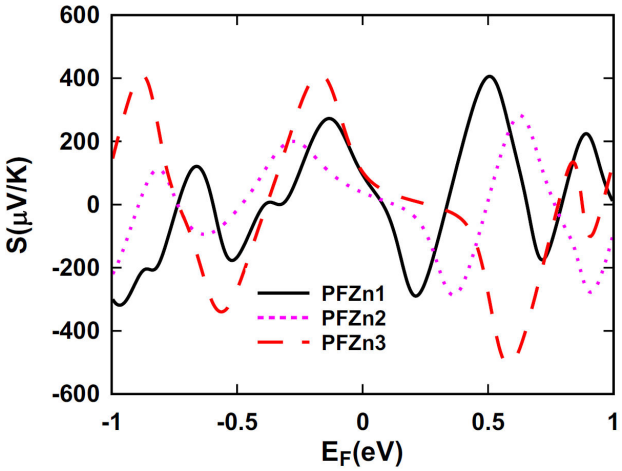

FIGURE 10. Figure 1b) presents the Seebeck coefficient S as a function of energy for a single zinc ion in the center of the porphyrin dimer molecular structures.

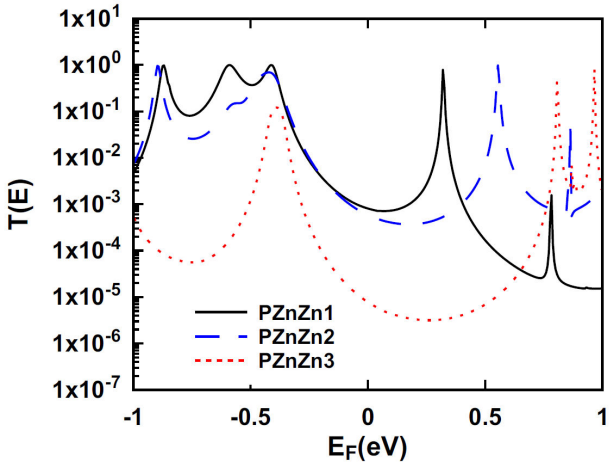

FIGURE 12. The electronic transmission coefficients as a function of energy for all two zinc ion in the centre of the porphyrin dimer molecular structures are presented in Fig. 1c).

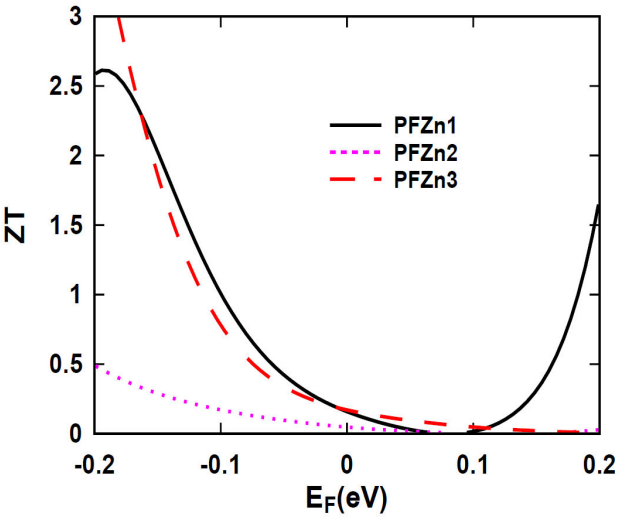

FIGURE 11. The electronic figure of merit ZT as a function of one zinc ion in the center of porphyrin dimer molecular structures is presented in Fig. 1b).

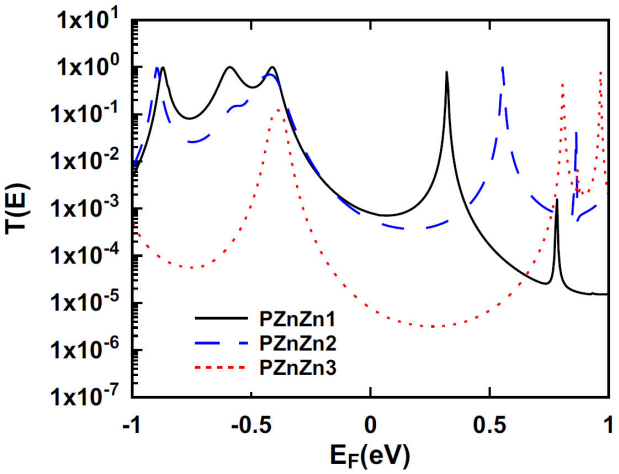

FIGURE 13. The electrical conductance as a function of energy for all two zinc ion in the center of the porphyrin dimer molecular structures is presented in Fig. 1c).

Seebeck coefficients, making them promising for thermoelectric applications.

For all one zinc ion in the center of the porphyrin dimer molecular structures in Fig. 1b). Figure 11 shows the electronic figure of merit ZT over a range of Fermi energies at room temperature for each one. Due to the fluctuating value of electrical conductance G, electronic thermal conductance K, and Seebeck coefficient S Fig. 11 shows very close values of the electronic figure of merit ZT of structures (PFZn1) and (PFZn3) are highest. The figure of merit ZT of structure ethynyl-linked porphyrin dimer with one zinc ion (PFZn2) is the lowest because S is the lowest.

In the third part of this work, using the same structures that were used in the previous section, we investigate the impact of changing the type of linker between porphyrin dimer units and the two zinc atoms in the center of porphyrin on electronic and thermoelectric properties in the different three-linker porphyrin dimers, as shown in Fig. 1c).

Figure 12 shows the effect of the transmission coefficient $T(E)$ as a function of energy for three different linked porphyrin dimers. The appearance of two zinc ion in the centre of porphyrin dimers has a remarkable effect on the transmission coefficient, particularly around Fermi energy. The gradual appearance of zinc ions in the center of porphyrin dimer units leads to shifting the peaks of the transmission coefficient away from the Fermi energy. (black, blue dashed, and red dotted line).

Figure 13 shows that the electrical conductance decreased with the appearance of two zinc atoms in the center of the porphyrin dimer units and three different linkers. Figure 13 shows that moving from a (PZnZn1) (black line) and (PZnZn3) (pink dotted line) to (PZnZn2) (red dashed line) leads to an apparent decrease in electrical conductance around the Fermi energy in a wide range of energies. The

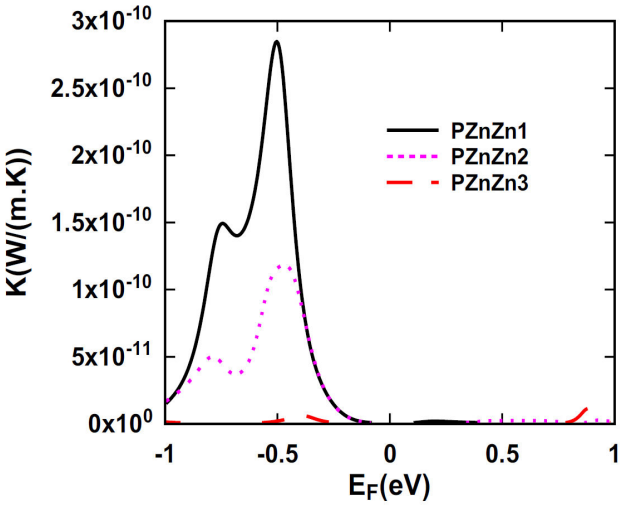

FIGURE 14. The electronic thermal conductivity as a function of energy for all two zinc ion in the center of the porphyrin dimer molecular structures is presented in Fig. 1c).

energy transfer rates in directlylinked and phenyl-linked porphyrin dimers are notably rapid, facilitating efficient charge transport.

The electronic thermal conductivity for a range of Fermi energies at room temperature all two zinc ion in the center of porphyrin dimer molecular structures is presented in Fig. 1c). is shown in Fig. 14. The curves of the electronic thermal conductivity of all structures (PZnZn1), (PZnZn2), and (PZnZn3) are very close, particularly around Fermi energy, showing that the electronic thermal conductivity decreased with the appearance of different three-linker tow zinc atoms in porphyrin dimer units. Different linkers, such as ethynyl and phenyl, affect the degree of electronic communication between porphyrin units due to changes in vibrational modes and reduced electronic pathways, leading to lower thermal conductance.

Figure 15 shows the Seebeck coefficient S over a range of Fermi energies at room temperature for each of the two zinc ion in the center of the porphyrin dimer molecular structures,

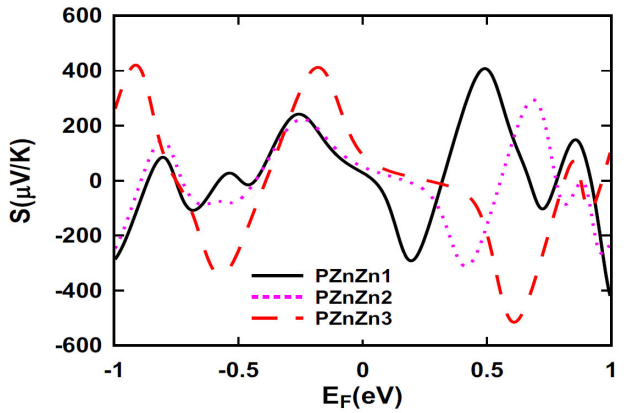

FIGURE 15. The Seebeck coefficient S as a function of energy for all two zinc ion in the center of the porphyrin dimer molecular structures is presented in Fig. 1c).

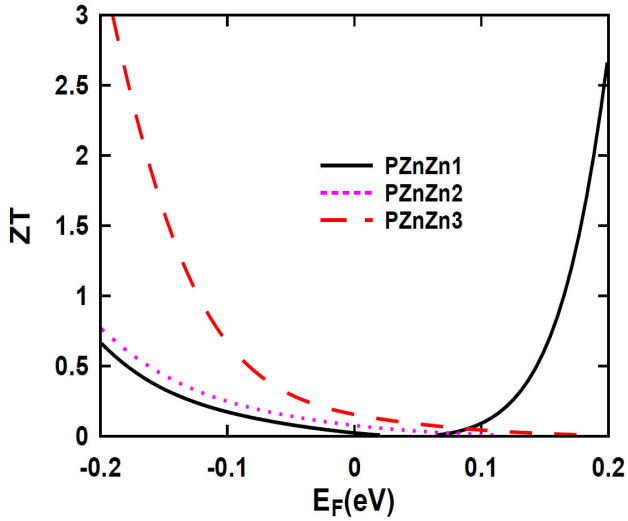

FIGURE 16. The electronic figure of merit ZT as a function of energy for all two zinc ion in the center of the porphyrin dimer molecular structures is presented in Fig. 1c).

as presented in Fig. 1c). Figure 15 demonstrates that the appearance of the two zinc ion at the center of the different three-linked porphyrin dimers affects the Seebeck coefficient S. Figure 15 shows that Seebeck coefficient curves of that moving from a (PZnZn3) (red dash line) to (PZnZn1) (black line) lead to clear different values in electrical conductance around Fermi energy in a wide range of energies, particularly around Fermi energy in energy windows of -0.5 to $+0.5$ eV.

The presence of organic radicals in (PZnZn3) leads to enhanced electronic conductance, and quantum interference exhibits high Seebeck coefficients due to its unique electronic properties and structural characteristics. The combination of radical effects and quantum interference significantly enhances its thermoelectric performance.

Figure 16 shows the electronic figure of merit ZT over a range of Fermi energies at room temperature for all different three-linked two zinc ion in the center of porphyrin dimers in Fig. 1c). Figure 16 shows that the ZT values of of that moving from a (PZnZn3) (red dash line) to (PZnZn1) (black line) lead to clear different values in electrical conductance around Fermi energy in a wide range of energies, particularly around Fermi energy in energy windows of -0.2 to +0.2 eV.

4. Conclusion

This work has compared the electronic and thermoelectric properties of three different families of porphyrin dimers. Our calculations perfectly focused on the correlation center of these three zinc porphyrin dimer families and electronic and thermoelectric properties. The result demonstrates that in the free-based porphyrin dimer family, all electronic and thermoelectric properties-transmission coefficient, electrical conductance G, thermal conductivity K, thermopower S, and figure of merit ZT have been affected by the changing of three different linkers between porphyrin dimers. In the second

part of the one zinc ion in the center porphyrin dimer families and the third part of the two zinc ion in the center porphyrin dimer families, the result demonstrates that the electrical and thermal conductances are highly affected by the presence of a phenyl-linked of these dimers. The appearance of a zinc atom leads to a significant decrease in electronic and thermal conductance. On the other hand, the thermopower of all other structures shows no noticeable change, especially around the Fermi energy. Therefore, the gradual appearance of different linkers between porphyrin dimer units plays an essential role in electronic and thermal properties. Structures that show the highest figure of merit ZT are the free-based phenyl-linked porphyrin dimer (PF3), the phenyl-linked porphyrin dimer with one zinc ion (PFZn3), and the phenyl-linked porphyrin dimer with two zinc ion (PZnZn3). This means the best results are the phenyl-linked porphyrin dimer. So, we believe such results will strongly help enhance thermoelectric materials' fast and trustworthy design.

Acknowledgments

We are extremely grateful to the University of Thi-Qar, College of Science, Department of Physics, for providing us with the facilities and necessary resources to carry out our research activities smoothly.

1. P. Reddy, S. Y. Jang, R. A. Segalman, A. Majumdar, Thermoelectricity in molecular junctions. *Science.* **315** (2007) 1568-71. https://doi.org/10.1126/science.1137149
2. L. Cui, R. Miao, C. Jiang, E. Mehofer, P. Reddy, Perspective: Thermal and thermoelectric transport in molecular junctions. *J Chemical Physics.* **146** (2017) 092201. https://doi.org/10.1063/1.4976982
3. H. Xu *et al.*, Electrical Conductance and Thermopower of β-Substituted Porphyrin Molecular Junctions- Synthesis and Transport. *J. American Chemical Society,* **145** (2023) 23541-23555. https://doi.org/10.1021/jacs.3c07258
4. J. Jang, P. He, H. Yoon. Molecular thermoelectricity in EGaIn-based molecular junctions. *Accounts of Chemical Research*. **56** (2023) 1613-1622. https://doi.org/10.1021/acs.accounts.3c00168
5. M. Di Domenico, I. Carlomagno, A. Sellitto, Wave propagation at nano-scale in coupled transport phenomena: application to thermoelectricity. *Meccanica,* **59** (2024) 1685-1701. https://doi.org/10.1007/s11012-024-01777-3
6. M. Samanta, S. Kundu, D. Mitra, Thermoelectric Effects. *Thermoelectric Polymers: Properties and Applications*, **162** (2024) 1-23. ISBN: 978-1-64490-300-1.
7. D. Cotfas, A. Enesca, P. Cotfas. Enhancing the performance of the solar thermoelectric generator in unconcentrated and concentrated light. *Renewable Energy*, **221** (2024) 119831. https://doi.org/10.1016/j.renene.2023.119831
8. D. Luo, Y. Yan, W. Chen, B. Cao. Exploring the dynamic characteristics of thermoelectric generator under fluctuations of exhaust heat. *International Journal of Heat and Mass Transfer*, **222** (2024) 125151. https://doi.org/10.1016/j.ijheatmasstransfer.2023.125151
9. W. Yang *et al.*, Taguchi optimization and thermoelectrical analysis of a pin fin annular thermoelectric generator for automotive waste heat recovery. *Renewable Energy*, **220** (2024) 119628. https://doi.org/10.1016/j.renene.2023.119628
10. D. Yousri, A. Fathy, H. Farag, E. El-Saadany. Optimal dynamic reconfiguration of thermoelectric generator array using RIME optimizer to maximize the generated power. *Applied Thermal Engineering*, **238** (2024) 122174. https://doi.org/10.1016/j.applthermaleng.2023.122174
11. P. Alegría, L. Catalan, M. Araiz, I. Erro, D. Astrain. Design and optimization of thermoelectric generators for harnessing geothermal anomalies: A computational model and validation with experimental field results. *Applied Thermal Engineering*, **236** (2024) 121364. https://doi.org/10.1016/j.applthermaleng.2023.121364
12. R. E. Dong *et al.*, Numerical modeling of a novel hybrid system composed of tubiform solid oxide fuel cell and segmented annular thermoelectric generator (SOFC/SATEG). *Applied Thermal Engineering*, **243** (2024) 122706. https://doi.org/10.1016/j.applthermaleng.2024.122706
13. T. J. Seebeck, A. Octtingen, Magnetische polarisation der metalle und erze durch temperatur-differenz. (1895) Leipzig: W. Engelmann.
14. T. Bennett, Synthesis and characterisation of novel molecular wires for studies of thermoelectricity. PhD thesis, (2022), Imperial College London. UK. https://doi.org/10.25560/99865
15. O. Albeydani, Theoretical study of vertical van der Walls metal-porphyrin and metal free-porphyrin junctions. *Physica Scripta.* **98** (2023) 085403. https://doi.org/10.1088/1402-4896/ace222
16. A. Al-Jobory, M. Noori, Thermoelectric properties of metallocene derivative single-molecule junctions. *J Electronic Materials*, **49** (2020) 5455-5459. https://doi.org/10.1007/s11664-020-08279-4
17. W. Ma, Preparation and performance analysis of electrochemically assisted molecular electronic devices. *International Journal of Electrochemical Science*, **19** (2024) 100489. https://doi.org/10.1016/j.ijoes.2024.100489
18. D. Vuillaume, Beyond-CMOS: state of the art and trends. Molecular Electronics: Electron, (2023) 251. ISBN: 978-1-394-22870-6
19. M. Yuan, Y. Qiu, H. Gao, J. Feng, Y. Wu, Molecular electronics: from nanostructure assembly to device integration. *J American Chemical Society,* **146** (2024) 7885-7904. https://doi.org/10.1021/jacs.3c14044

20. C. Yan *et al.*, From Molecular Electronics to Molecular Intelligence. *ACS nano*, **18** (2024) 28531-28556. https://doi.org/10.1021/acsnano.4c10389

21. B. Yadav, M. Ravikanth. Porphyrinoid framework embedded with polycyclic aromatic hydrocarbons: new synthetic marvels. *Organic & Biomolecular Chemistry*, **22** (2024) 1932-1960. https://doi.org/10.1039/D3OB02116E

22. F. Santanni, A. Privitera. Metalloporphyrins as building blocks for quantum information science. *Advanced Optical Materials*, **12** (2024) 2303036. https://doi.org/10.1002/adom.202303036

23. M. Noori *et al.*, Tuning the electrical conductance of metalloporphyrin supramolecular wires. *Sci Rep.* **6** (2016) 37352. https://doi.org/10.1038/srep37352

24. M. Mathius, Synthesis of Highly Conjugated Porphyrinoid Systems. Master thesis, (2022). Illinois State University. *United States.* https://doi.org/10.30707/ETD2022.20221020070312747424.999980

25. A. S. Estrada-Montaño *et al.*, Metalloporphyrins: Ideal catalysts for olefin epoxidations. *J Porphyrins and Phthalocyanines*, **26** (2022) 821-836. https://doi.org/10.1142/S1088424622300051

26. V. Singh, P. Thakur, V. Ganesan, M. Sanker.Zn (II) porphyrin-based polymer facilitated electrochemical synthesis of green hydrogen peroxide. *Journal of Electroanalytical Chemistry*, **919** (2022) 116536. https://doi.org/10.1016/j.jelechem.2022.116536

27. C. Hahn da Silveira, A. Otavio, C. Amanda, M. Nathalia, L. Costa, A. Bernaldo, Synthesis, photophysics, computational approaches, and biomolecule interactive studies of metalloporphyrins containing pyrenyl units: Influence of the metal center. *European J Inorganic Chemistry*, **(12)** (2022) e202200075. https://doi.org/10.1002/ejic.202200075

28. N. Magdaong *et al.*, Photophysical Properties and Electronic Structure of Zinc(II) Porphyrins Bearing 0-4 meso-Phenyl Substituents: Zinc Porphine to Zinc Tetraphenylporphyrin (ZnTPP). *J Phys Chem A.* **124** (2020) 7776-7794. https://doi.org/10.1021/acs.jpca.0c0684

29. Y. F. Liu, M. Juan, S. Kristian, Computational investigation of acene-modified zinc-porphyrin based sensitizers for dye-sensitized solar cells. *J Physical Chemistry C*, **119** (2015) 8417-8430. https://doi.org/10.1039/C3CP54050B

30. X. Yu *et al.*, A new A3B zinc (II)-porphyrin ligand and its ruthenium (II) complex: Synthesis, photophysical properties and photocatalytic applications. *J Molecular Structure*, **1237** (2021) 130358. https://doi.org/10.1016/j.molstruc.2021.130358

31. P. J. Low, S. Marqués-González,, Molecular wires: an overview of the building blocks of molecular electronics. Single-Molecule Electronics: An Introduction to Synthesis, *Measurement and Theory*, (2016) 87-116. https://doi.org/10.1007/978-981-10-0724-8

32. A. Al-mebir, S. AL-Saidi, Tuning Optoelectronic Properties of Double Quantum Dot Structure Using Tight-Binding Model for Photo-Electric Applications. *NeuroQuantology*, **19** (2021) 1. https://doi.org/10.14704/nq.2021.19.3.NQ21021

33. S. AL-Saidi, A. Al-mebir, Asymmetric Double Quantum Dot Structure as Nanoscale Diode. *University of Thi-Qar J*, **13** (2018) 1-17. https://jutq.utq.edu.iq/index.php/main/article/view/151

34. A. Al-mebir, S. Al-Saidi, Theoretical Investigation of Base Pairs-Dependent Electron Transport in DNA System. in Journal of Physics: Conference Series. *J. Phys.: Conf. Ser.* **1530** (2020) 012147. https://doi.org/10.1088/1742-6596/1530/1/012147

35. S. Al-Saidi, A. Al-mebir, Electronic Properties Simulation of Guanine Molecule. in Journal of Physics: Conference Series. *IOP Publishing. J. Phys.: Conf. Ser.* **1530** (2020) 012148. https://doi.org/10.1088/1742-6596/1530/1/012148

36. S. Ke, H. Baranger, W. Yang, Models of electrodes and contacts in molecular electronics. *J chemical physics*, **123** (2005) 114701. https://doi.org/10.1063/1.1993558

37. G. Schull, T. Frederiksen, A. Arnau, D. Sánchez-Portal, R. Berndt, Atomic-scale engineering of electrodes for single-molecule contacts. *Nat Nanotechnol.* **6** (2011) 23-7. https://doi.org/10.1038/nnano.2010.215

38. Z. Liu, S. Ren, X. Guo, Switching effects in molecular electronic devices. *Molecular-Scale Electronics: Current Status and Perspectives*, (2019) 173-205. https://doi.org/10.1007/978-3-030-03305-7_6

39. S. AL-Saidi, A. Al-mebir, M. Hallool, Characteristics of Thymine Molecule System Behave as Molecular Electronic Device. *Misan Journal of Academic Studies (Humanities and social sciences)*, **18** (2019) 130-143. https://www.misan-jas.com/index.php/ojs/article/view/55

40. M. Noori, H. Sadeghi, C. Lambert, High-performance thermoelectricity in edge-over-edge zinc-porphyrin molecular wires. *Nanoscale*, **9** (2017) 5299-5304. https://doi.org/10.1039/C6NR09598D

41. M. Noori, H. Sadeghi, Q. AlGhaliby, S. Bailey, C. Lambert, High cross-plane thermoelectric performance of metalloporphyrin molecular junctions. *Physical Chemistry Chemical Physics*, **19** (2017) 17356-17359. https://doi.org/10.1039/C7CP02229H

42. E. Leary *et al.*, Detecting Mechanochemical Atropisomerization within an STM Break Junction. *J Am Chem Soc.* **140** (2018) 710-718. https://doi.org/10.1021/jacs.7b10542

43. M. Noori, Quantum Theory of Electron Transport Through Photo-Synthetic Porphyrins. PhD thesis, (2017) Lancaster University, United Kingdom.

44. D. Preesam, H. Milani Moghaddam, M. Noori, Enhanced thermoelectric properties of zinc porphyrin dimers-based molecular devices. *The European Physical J D*, **78** (2024) 1-5. https://doi.org/10.1140/epjd/s10053-024-00932-5

45. D. Preesam, M. Noori, H. Moghaddam, The Effect of Linker Group on Thermoelectric Properties of Dimer Zinc Porphyrin-Based Molecular Junctions. *University of Thi-Qar Journal of Science*, **10** (2023) 177-180, https://doi.org/10.32792/utq/utjsci/v10i2.1133

46. A. Berlicka *et al.*, 21-Carba-23-selenaporphyrinoid Dyads-An Azepine Unit as a Merging Motif. *Angew Chem Int Ed Engl.* **63** (2024) e202314925, https://doi.org/10.1002/anie.202314925.

47. T. Higashino, Y. Kurumisawa, H. Iiyama, H. Imahori, ABC-ABC-Type Directly meso-meso Linked Porphyrin Dimers. *Chemistry.* **25** (2019) 538-547, https://doi.org/10.1002/chem.201805405

48. Y. Liu *et al.*, Ethynyl-linked push-pull porphyrin hetero-dimers for near-IR dye-sensitized solar cells: photovoltaic performances versus excited-state dynamics. *Physical Chemistry Chemical Physics,* **14** (2012) 16703-16712, https://doi.org/10.1039/C2CP43165C

49. T. Hamamura *et al.*, Dye-sensitized solar cells using ethynyl-linked porphyrin trimers. *Physical Chemistry Chemical Physics,* **16** (2014) 4551-4560. https://doi.org/10.1039/C3CP55184A

50. V. Tyurin, A. Shkirdova, O. Koifman, I. Zamilatskov. Meso-Formyl, Vinyl, and Ethynyl Porphyrins-Multipotent Synthons for Obtaining a Diverse Array of Functional Derivatives. *Molecules.* **28** (2023) 5782. https://doi.org/10.3390/molecules28155782.

51. M. Gilbert, B. Albinsson, Photoinduced charge and energy transfer in molecular wires. *Chemical Society Reviews,* **44** (2015) 845-862. https://doi.org/10.1039/C4CS00221K

52. Y. Liu *et al.*, N-fused carbazole-zinc porphyrin-free-base porphyrin triad for efficient near-IR dye-sensitized solar cells. *Chem Commun (Camb).* **47** (2011) 4010-2. https://doi.org/10.1039/c0cc03306e

53. X. Li *et al.*, The Role of Porphyrin-Free-Base in the Electronic Structures and Related Properties of N-Fused Carbazole-Zinc Porphyrin Dye Sensitizers. *Int J Mol Sci.* **16** (2015) 27707-20. https://doi.org/10.3390/ijms161126057.

54. M. Cohen Jungerman, S. Shmueli, P. Shekhter, Y. Selzer, Unusually High Thermopower in Molecular Junctions from Molecularly Induced Quantized States in Their Semimetal Leads. *Nano Lett.* **25** (2025) 2756-2762. https://doi.org/10.1021/acs.nanolett.4c05852.

55. H. Nguyen, T. Ono, Electron-transport properties of ethyne-bridged diphenyl zinc-porphyrin molecules. *Japanese J Applied Physics,* **54** (2015) 055201, https://doi.org/10.48550/arXiv.1501.01365

56. M. N. Borges-Martinez, Montenegro-Pohlhammer, and G. Cardenas-Jiron, The bimetallic and the anchoring group effects on both optical and charge transport properties of hexaphyrin amethyrin. *New Journal of Chemistry*, **45** (2021) 6521-6534, https://doi.org/10.1039/D1NJ00091H

57. Z. Dunn, M. Hammer, B. Tobham, T. Perrine, Linker Effects in Porphyrin Polymeric Donor Materials for Photovoltaic Devices. *J Physical Chemistry C,* **121** (2017) 12018-12024. https://doi.org/10.1021/ACS.JPCC.7B02682

58. S. Kopp *et al.*, Charge and Spin Transfer Dynamics in a Weakly Coupled Porphyrin Dimer. *J Am Chem Soc.* **146** (2024) 21476-21489, https://doi.org/10.1021/jacs.4c04186